J Mater Sci (2008) 43:2611–2617
DOI 10.1007/s10853-008-2470-z

A thermodynamic description of the melting process in nanometer-sized particles

Francesco Delogu

Received: 13 June 2007 / Accepted: 14 January 2008 / Published online: 20 February 2008

Abstract The melting behavior of nanometer-sized Sn particles with radius in the range between 5 and 50 nm is analyzed within the conceptual framework of classical thermodynamics. Experimentally observed size-dependent melting points and latent heats of fusion are exploited to point out the occurrence of pre-melting phenomena at the particle surface. The size-dependent values of the thermodynamic state functions associated with the solid–liquid interface are estimated together with the thickness of the interface layer.

Introduction

Physical and chemical systems in the size domain between clusters and infinite coarse-grained materials are characterized by a high surface-to-volume ratio [1–3]. A substantial fraction of atoms and molecules lies then at, or close to, the surface. Correspondingly, surface energy gives a significant contribution to the overall free energy of such systems [1–3]. This induces a change of physical and chemical properties, which can be described by relatively simple scaling equations involving a power-law dependence on the system size [2–4]. Such smooth size effects can be in principle exploited to obtain information on the fundamental thermodynamics underlying the observed phenomenology. Within such conceptual framework, this work specifically addresses the well-known melting point depression of nanometer-sized metallic particles.

F. Delogu (✉)
Dipartimento di Ingegneria Chimica e Materiali, Università di Cagliari, piazza d'Armi, Cagliari 09123, Italy
e-mail: delogu@dicm.unica.it

The phenomenon, theoretically predicted since the 1970s of the XIX century [5] and extensively studied later [6–10], essentially consists of the decrease of the melting point as the particle size decreases. Such behavior is successfully described by several phenomenological models, which generally invoke a size dependence of the chemical potential [6, 11–15]. As shown by the modeling approaches developed in the years, the problem is intimately intertwined with the one of surface pre-melting [16]. The solid–liquid phase transformation is indeed related alternatively either to the formation of a molten layer covering the particle surface below its melting point or to the heterogeneous nucleation of a transition front traveling from the surface inward at the melting point [6, 11–15]. The present work shows how a reliable discrimination between the two different melting scenarios can be obtained when the size dependence of the latent heat of fusion is also taken into account. It therefore reasserts the importance of accurate calorimetric measurements [17–20] for a comprehensive understanding of the thermodynamics of nanometer-sized systems.

Thermodynamic model

The present study focuses on the calorimetric measurements performed on Sn particles with radius r approximately in the range between 5 and 50 nm [17]. The experimental values quoted in Fig. 1a, b reveal that melting points T_m and latent heats of fusion $\Delta H_m^{exp}(T_m)$ undergo a substantial decrease as the radius r decreases. The depression of the latent heats of fusion $\Delta H_m^{exp}(T_m)$ immediately suggests the existence of a highly disordered surface layer which does not contribute to the final melting event at T_m [17, 21]. It follows that the decrease of

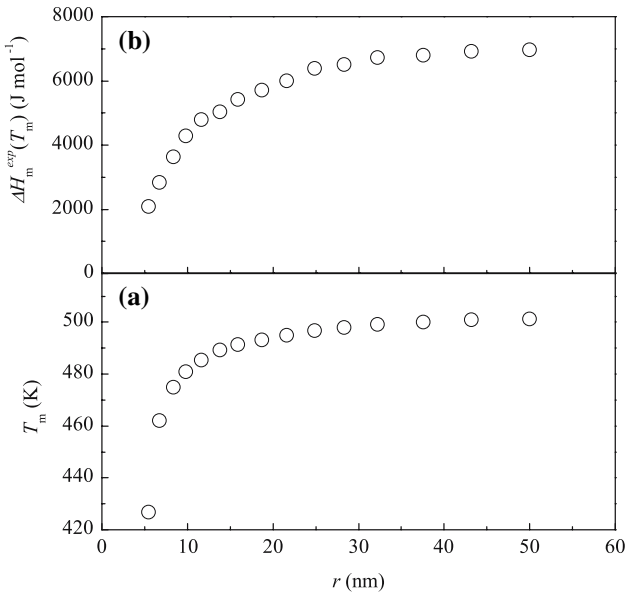

Fig. 1 (**a**) The experimentally observed melting point T_m and (**b**) the latent heat of fusion $\Delta H_m^{exp}(T_m)$ as a function of the particle radius r

$\Delta H_m^{exp}(T_m)$ can be regarded as an indirect evidence of the occurrence of pre-melting phenomena at surfaces. However, a more detailed analysis of the thermodynamic behavior of nanometer-sized Sn particles opens the door to a sounder rationalization of experimental observations.

Let us consider the two melting scenarios schematically illustrated in Fig. 2. In the simplest case, melting occurs in one stage and the solid particle transforms at T_m into a liquid one. Under such conditions, the equality of their Gibbs free energies implies that

$$\frac{4}{3}\pi r^3\rho_s\Delta G_s(T_m) + 4\pi r^2\gamma_{sv}(T_m) = \frac{4}{3}\pi r^3\rho_l\Delta G_l(T_m) + 4\pi r^2\gamma_{lv}(T_m). \quad (1)$$

In the expression above $\Delta G_s(T_m)$ and $\Delta G_l(T_m)$ represent, respectively, the Gibbs free energies of solid and liquid phases at T_m, whereas $\gamma_{sv}(T_m)$ and $\gamma_{lv}(T_m)$ are the free energies of solid–vapor and liquid–vapor interfaces. Finally, ρ_s and ρ_l are the molar densities of solid and liquid phases. Equation 1 can be readily rearranged to

$$\frac{1}{3}r[\rho_l\Delta G_l(T_m) - \rho_s\Delta G_s(T_m)] = \gamma_{sv}(T_m) - \gamma_{lv}(T_m), \quad (2)$$

which points out the relationship between Gibbs and interface free energies at melting.

The second scenario regards instead a two-stage melting process involving first the occurrence of pre-melting phenomena at the particle surface and then the melting of the particle bulk. Under the assumption that only a surface layer of thickness δ is involved in pre-melting, the equality of Gibbs free energies for the second stage of the melting process leads to the following equation:

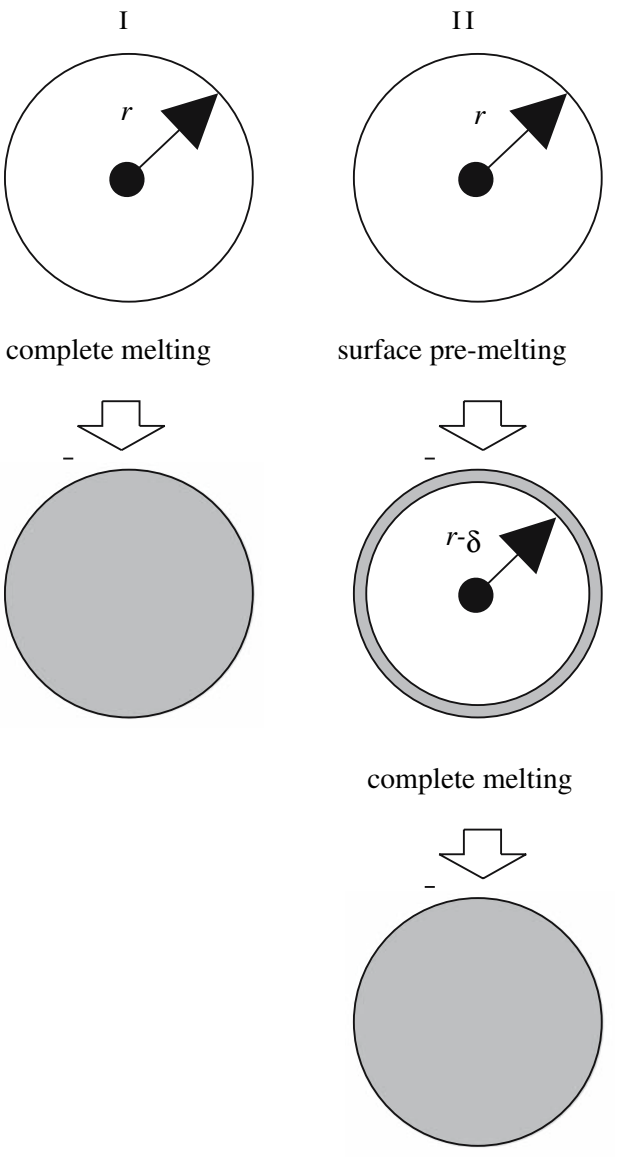

Fig. 2 Schematic cross-sectional view of a spherical particle in single-stage (left, I) and two-stage (right, II) heterogeneous melting scenarios. Light gray indicates the liquid phase

$$\frac{4}{3}\pi(r-\delta)^3\rho_s\Delta G_s(T_m) + 4\pi(r-\delta)^2\gamma_{sl}(T_m) + \frac{4}{3}\pi\left[r^3 - (r-\delta)^3\right]\rho_l\Delta G_l(T_m) + 4\pi r^2\gamma_{lv}(T_m) = \frac{4}{3}\pi r^3\rho_l\Delta G_l(T_m) + 4\pi r^2\gamma_{lv}(T_m) \quad (3)$$

It follows from simple algebraic manipulations that

$$\frac{1}{3}(r-\delta)[\rho_l\Delta G_l(T_m) - \rho_s\Delta G_s(T_m)] = \gamma_{sl}(T_m), \quad (4)$$

where $\gamma_{sv}(T_m)$ represents the free energy of the solid–liquid interface.

The thickness δ of the surface layer involved in pre-melting phenomena has been evaluated in previous work

starting from the comparison between the experimental latent heat of fusion $\Delta H_m^{exp}(T_m)$ and the expected enthalpy difference $\Delta H_l(T_m) - \Delta H_s(T_m)$ between the liquid phase and the bulk solid at the melting temperature T_m [21]. The δ values obtained are reported in Fig. 3 as a function of the particle size.

The difference $\rho_l \Delta G_l(T_m) - \rho_s \Delta G_s(T_m)$ can be easily evaluated from tabulated thermodynamic values [22] and the $\gamma_{sv}(T_m) - \gamma_{lv}(T_m)$ and $\gamma_{sl}(T_m)$ values estimated by means of Eqs. 2 and 4. At least at relatively large radii, the difference $\gamma_{sv}(T_m) - \gamma_{lv}(T_m)$ should be approximately equal to 130 mJ m^{-2}, as $\gamma_{sv}(T_m)$ and $\gamma_{lv}(T_m)$ are equal to about 680 and 550 mJ m^{-2}, respectively [23]. The free energy $\gamma_{sl}(T_m)$ of the solid–liquid interface roughly amounts instead to 55 mJ m^{-2} [23]. For the biggest particles, $\gamma_{sv}(T_m) - \gamma_{lv}(T_m)$ should be therefore approximately twice $\gamma_{sl}(T_m)$. The difference between the two cases is such that a discrimination between the single- and two-stage melting scenarios is possible despite the experimental uncertainties affecting the thermodynamic properties considered. To this aim, the product between one third of the particle radius r and the difference $\rho_l \Delta G_l(T_m) - \rho_s \Delta G_s(T_m)$ must be evaluated. According to the single-stage melting scenario, it is a measure of the difference $\gamma_{sv}(T_m) - \gamma_{lv}(T_m)$ between the free energies of solid–vapor and liquid–vapor interfaces and should approach at large radii the value of 130 mJ m^{-2}. Conversely, within the two-stage melting scenario it is roughly equal to the free energy $\gamma_{sl}(T_m)$ of the solid–liquid interface and should approach a value of about 55 mJ m^{-2}.

The results of calculations are reported in Fig. 4 as a function of the particle radius r. Data are quite scattered, probably due to experimental uncertainties affecting experimental findings. A general trend can be nevertheless identified. In particular, it can be seen that the values quoted are approximately equal to 53 mJ m^{-2} for particle radii roughly above 30 nm. A progressive increase is instead observed as the particle size decreases roughly from 30 to 10 nm. The values obtained for particle radii above 30 nm support therefore the two-stage melting scenario, which involves the occurrence of pre-melting processes at the particle surface at a temperature T_{pm} below the particle melting point T_m. The increase of plotted values from about 50 to 95 mJ m^{-2} at radii between 30 and 10 nm indicates in addition a marked rise of the solid–liquid interface energy at large surface curvatures. It is worth noting that temperature effects can not be considered responsible for the observed increase, being the particle melting points T_m lower as the particle radius r is smaller.

The knowledge of both surface layer thickness δ and solid–liquid interface free energy $\gamma_{sl}(T_m)$ make a rough estimate of the surface layer pre-melting temperature T_{pm} possible under the assumption that the difference $\gamma_{sv}(T_m) - \gamma_{lv}(T_m)$ between solid–vapor and liquid–vapor interface free energies remains approximately constant at 130 mJ m^{-2}. The relationship between all the thermodynamic quantities involved is provided by the equation

$$\frac{4}{3}\pi\left[r^3 - (r-\delta)^3\right]\left[\rho_l \Delta G_l(T_{pm}) - \rho_s \Delta G_s(T_{pm})\right] = 4\pi r^2[\gamma_{sv}(T_m) - \gamma_{lv}(T_m)] + 4\pi(r-\delta)^2\gamma_{sl}(T_m), \quad (5)$$

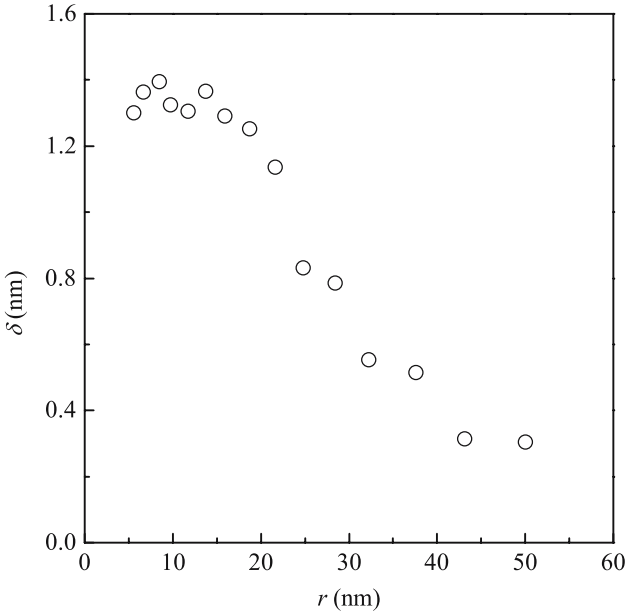

Fig. 3 The thickness δ of the molten surface layer as a function of the radius r of nanometer-sized particles

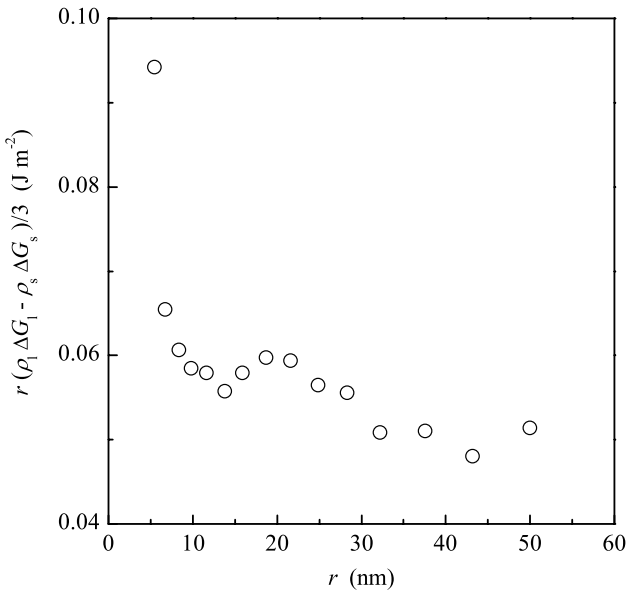

Fig. 4 The quantity $\frac{1}{3}r[\rho_l \Delta G_l(T_m) - \rho_s \Delta G_s(T_m)]$ as a function of the particle size r

which expresses the thermodynamic equilibrium condition for the solid–liquid transition of the surface layer of thickness δ. Pre-melting temperatures T_{pm} obtained from calculations are reported in Fig. 5 as a function of the particle radius r. The data exhibit a counterintuitive decreasing trend indicating that smaller particles undergo surface pre-melting phenomena at temperatures higher than the ones for larger particles. In other words, the assumption above leads to higher pre-melting points T_{pm} for smaller particle radii r giving rise to a curvature effect for pre-melting points T_{pm} opposite to the one observed in the case of melting points T_m. Far from being acceptable from a phenomenological point of view, the results of calculations on the temperatures T_{pm} at which a molten layer of thickness δ appears at the particle surface suggest a strong asymmetry in the smooth size effects affecting the solid–vapor and liquid–vapor interface free energies $\gamma_{sv}(T)$ and $\gamma_{lv}(T)$. Their difference $\gamma_{sv}(T_{pm}) - \gamma_{lv}(T_{pm})$ is indeed expected to define T_{pm} values that increase smoothly with the radius r in analogy with the observations concerning the particle size dependence of the melting point T_m. In particular, $\gamma_{sv}(T_{pm}) - \gamma_{lv}(T_{pm})$ is expected to increase above 130 mJ m^{-2}. Correspondingly, $\gamma_{sv}(T_{pm})$ is expected to grow with the surface curvature at rates larger than $\gamma_{lv}(T_{pm})$. The present data do not allow, however, any quantification of such effects.

Additional information on the thermodynamic properties of the nanometer-sized particles considered can be obtained by further manipulating Eq. 4. To such end, let us

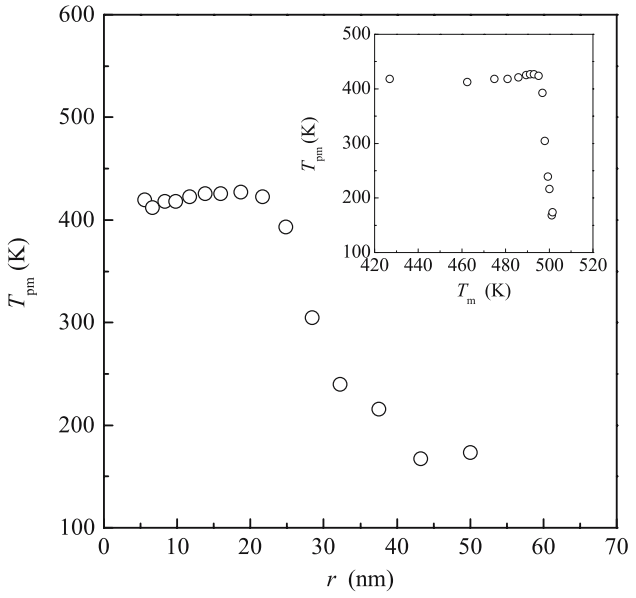

Fig. 5 The estimated pre-melting temperatures T_{pm} as a function of the particle radius r. The relationship between pre-melting temperatures T_{pm} and melting points T_m is illustrated in the inset

distinguish between enthalpic and entropic contributions to free energies. Equation 4 can be then re-formulated as

$$\frac{1}{3}(r-\delta)\{\rho_l\Delta H_l(T_m) - \rho_s\Delta H_s(T_m) - T_m[\rho_l\Delta S_l(T_m) - \rho_s\Delta S_s(T_m)]\} = h_{sl}(T_m) - T_m s_{sl}(T_m). \quad (6)$$

The quantities $\Delta H_l(T_m)$ and $\Delta H_s(T_m)$ represent, respectively, the enthalpies of the liquid and solid phases, whereas $\Delta S_l(T_m)$ and $\Delta S_s(T_m)$ correspond to their entropies. The terms $h_{sl}(T_m)$ and $s_{sl}(T_m)$ quantify, instead, the enthalpy and entropy associated with the free energy of the solid–liquid interface. Equation 6 can be rearranged to

$$\frac{4}{3}\pi(r-\delta)^3[\rho_l\Delta H_l(T_m) - \rho_s\Delta H_s(T_m)] - 4\pi(r-\delta)^2 h_{sl}(T_m) = T_m\left\{\frac{4}{3}\pi(r-\delta)^3[\rho_l\Delta S_l(T_m) - \rho_s\Delta S_s(T_m)] - 4\pi(r-\delta)^2 s_{sl}(T_m)\right\}. \quad (7)$$

The left-hand side of the expression above is equal to the total enthalpy change accompanying the particle melting. As indicated in the equation below,

$$\frac{4}{3}\pi(r-\delta)^3[\rho_l\Delta H_l(T_m) - \rho_s\Delta H_s(T_m)] - 4\pi(r-\delta)^2 h_{sl}(T_m) = \frac{4}{3}\pi r^3\rho_s\Delta H_m^{exp}(T_m), \quad (8)$$

it is related to the experimentally observed latent heat of fusion $\Delta H_m^{exp}(T_m)$. Equation 8 makes the generally accepted interpretation of the $\Delta H_m^{exp}(T_m)$ depression in terms of surface pre-melting [17, 21] less controversial. It should be noted indeed that the depression of $\Delta H_m^{exp}(T_m)$ with respect to the expected enthalpy difference $\Delta H_l(T_m) - \Delta H_s(T_m)$ between the liquid and solid phases at each temperature T_m naturally arises from the minus sign preceding the enthalpic contribution $h_{sl}(T_m)$ associated with the free energy $\gamma_{sl}(T_m)$ of the solid–liquid interface. The conceptual framework of the two-stage melting scenario is thus able to provide a satisfactory explanation of the decrease of $\Delta H_m^{exp}(T_m)$ values.

Equation 8 can be further manipulated to estimate the enthalpic content associated with the solid–liquid interface free energy

$$h_{sl}(T_m) = \frac{1}{3}(r-\delta)[\rho_l\Delta H_l(T_m) - \rho_s\Delta H_s(T_m)] - \frac{1}{3}r\rho_s\Delta H_m^{exp}(T_m). \quad (9)$$

Of course, a rough estimate of the entropy $s_{sl}(T_m)$ associated with the free energy of the solid–liquid interface at T_m becomes correspondingly possible. The $h_{sl}(T_m)$ and $s_{sl}(T_m)$ values resulting from calculations are shown in Fig. 6 as a function of the particle radius r. Both quantities display a significant increase as the particle size decreases. This

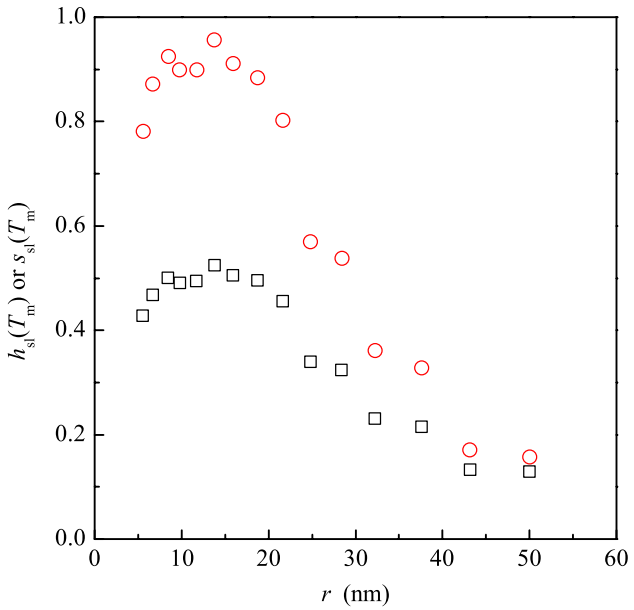

Fig. 6 The enthalpy $h_{sl}(T_m)$ (□, J mol^{-1} m^{-2}) and entropy $s_{sl}(T_m)$ (○, 10^3 J K^{-1} mol^{-1} m^{-2}) associated with the free energy $\gamma_{sl}(T_m)$ of the solid–liquid interface at T_m as a function of the particle radius r

suggests that both the energy content and the structural disorder of the solid–liquid interface are affected by smooth size effects and increase as the surface curvature increases.

It is worth noting here that the observed size dependence of both melting points T_m and latent heats of fusion $\Delta H_m^{exp}(T_m)$ has significant implications for the melting behavior of the nanometer-sized particles. Let us consider a particle with a spherical bulk region, i.e. a solid interior covered by a molten layer, of radius r_1 melting at $T_{m,1}$. Due to the presence of the solid–liquid interface the mechanism of solid–liquid transition is heterogeneous and the solid layer immediately below the solid–liquid interface is expected to melt before the remaining bulk region. Once such interface layer has melted, the solid bulk has a radius $r_2 < r_1$. It is therefore expected to melt at a temperature $T_{m,2} < T_{m,1}$ as a consequence of the known smooth size effects. This situation is different from the one characterizing the melting behavior of a system with a plane solid–liquid interface. In this latter case, the transition from the solid phase to the liquid one of a layer of a certain thickness below the plane solid–liquid interface does not change indeed the interface curvature. As a result, any given layer below the solid–liquid interface melts at the same temperature as the others independently of the amount of liquid phase covering the solid interior. Curvature effects on the melting points of nanometer-sized particles are expected to influence the propagation rates of the solid–liquid transition front. A detailed account of such effects will be given elsewhere.

The aforementioned $h_{sl}(T_m)$ and $s_{sl}(T_m)$ data can be further exploited to estimate the enthalpy $h_{s,i}(T_m)$ and the entropy $s_{s,i}(T_m)$ characterizing the layer of atomic species on the solid-phase side of the solid–liquid interface. To this end, the point regarding the way the free energy $\gamma_{sl}(T_m)$ is distributed at the solid–liquid interface should be addressed. In absence of specific information about such distribution, the free energy $\gamma_{sl}(T_m)$ is here assumed to affect only the solid-phase side of the interface. It then follows that the free energy $\gamma_{sl}(T_m)$, and then the enthalpic and entropic contents $h_{sl}(T_m)$ and $s_{sl}(T_m)$, can be attributed to the solid-phase side of the solid–liquid interface. Following this line, it is possible to suppose the existence of a layer of atomic species on the solid-phase side of the solid–liquid interface of thickness ξ bearing a free energy

$$g_{s,i}(T_m) = \frac{4}{3}\pi\left[(r-\delta)^3-(r-\delta-\xi)^3\right]\rho_s\Delta G_s(T_m) + 4\pi(r-\delta)^2\gamma_{sl}(T_m). \quad (10)$$

The thickness ξ of the solid–liquid interface on the solid-phase side can be tentatively estimated by applying a Kauzmann-like criterion based on the entropy content of a given volume of crystalline solid [24, 25]. Following the original criterion, it is very unlikely that the entropy of a given volume of solid could become larger than the one pertaining to the same volume of liquid phase without a significant modification of its structural arrangement [24, 25]. In the present case, such criterion could be interpreted as a constraint on the entropy content $s_{s,i}(T_m)$ of the solid–liquid interface layer on the solid-phase side such that $s_{s,i}(T_m)$ must be either smaller or equal to the corresponding entropy of the liquid phase $\Delta S_l(T_m)$ at the same temperature T_m. It follows that

$$\frac{4}{3}\pi\left[(r-\delta)^3-(r-\delta-\xi)^3\right]\rho_s\Delta S_s(T_m) + 4\pi(r-\delta)^2 s_{sl}(T_m) \le \frac{4}{3}\pi\left[(r-\delta)^3-(r-\delta-\xi)^3\right]\rho_l\Delta S_l(T_m). \quad (11)$$

The left-hand side of the expression above represents the entropy content $s_{s,i}(T_m)$ of the solid–liquid interface layer of thickness ξ, whereas the right-hand side is the entropy of the same volume of liquid phase. As evident from Fig. 7, the entropy content $s_{s,i}(T_m)$ of the solid–liquid interface layer critically depends on the layer thickness ξ. In particular, $s_{s,i}(T_m)$ is larger than $\Delta S_l(T_m)$ at relatively small ξ values.

For each particle, the condition of equality between $s_{s,i}(T_m)$ and $\Delta S_l(T_m)$ permits to identify the minimum layer thickness ξ_{min} value satisfying the Kauzmann-like criterion proposed above. The ξ_{min} values obtained are reported in Fig. 8 as a function of the particle radius r. Quite surprisingly, they closely match the δ values representing the thickness of the molten layer formed at the particle surface

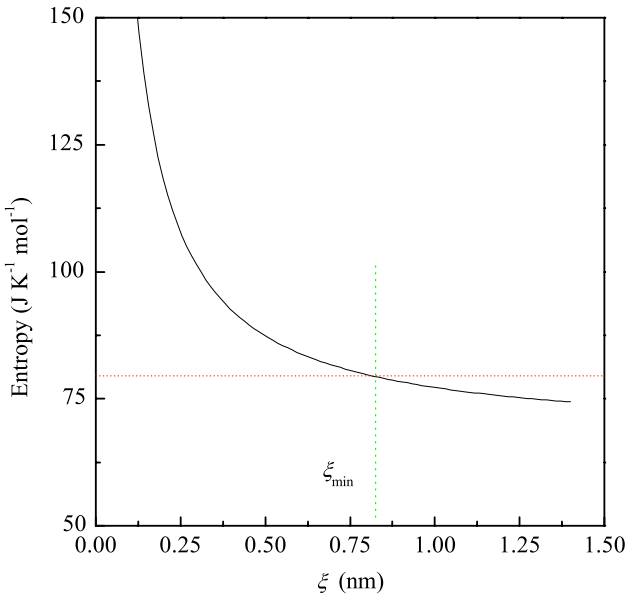

Fig. 7 The entropy $s_{s,i}(T_m)$ (solid line) of the layer on the solid-phase side of the solid–liquid interface as a function of the thickness layer ξ. The liquid phase entropy $\Delta S_l(T_m)$ is also quoted (horizontal dotted line). The vertical dotted line identifies the minimum solid–liquid interface layer thickness ξ_{min} satisfying the Kauzmann-like criterion

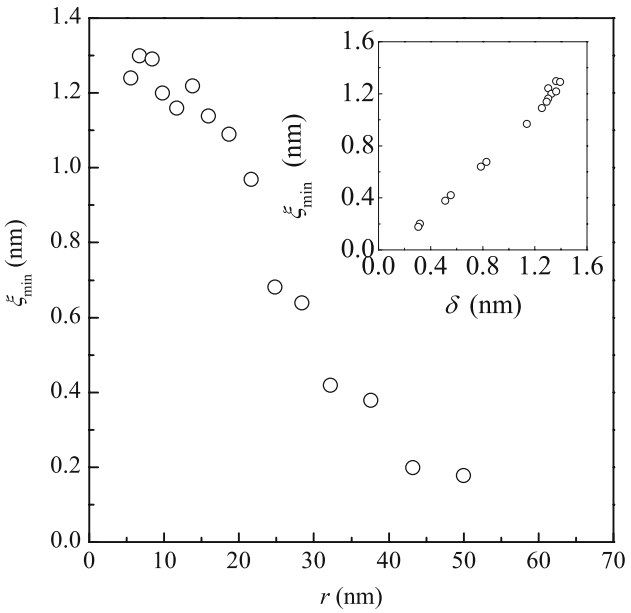

Fig. 8 The minimum solid–liquid interface layer thickness ξ_{min} satisfying the Kauzmann-like criterion as a function of the particle radius r. The inset quotes the ξ_{min} values as a function of the molten surface layer thickness δ

as a consequence of pre-melting phenomena and quoted in Fig. 3. The correspondence is further pointed out by the linear trend with almost unit slope, shown in the inset, obtained by quoting the ξ_{min} values as a function of the δ ones.

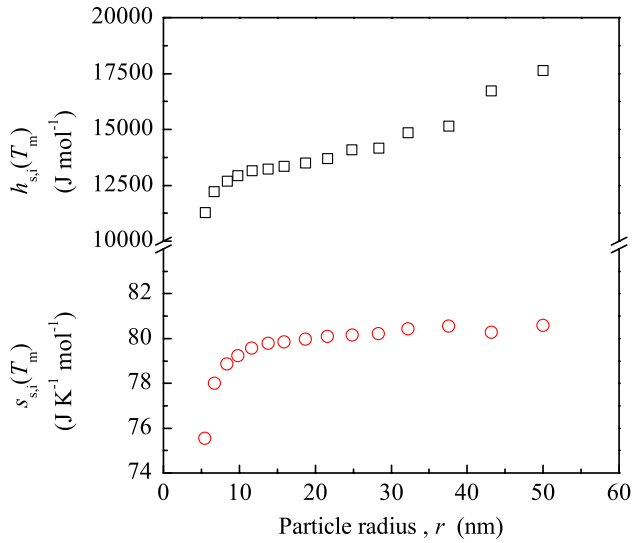

Fig. 9 The enthalpy $h_{s,i}(T_m)$ and the entropy $s_{s,i}(T_m)$ of the solid-phase side layer of thickness ξ_{min} at the solid–liquid interface as a function of the particle radius r

The data discussed in the present work are not sufficient to draw a definite conclusion about the thickness of the layer structurally and energetically perturbed as a consequence of its neighborhood to a solid–vapor or solid–liquid interface. It is however tempting to hypothesize that the thickness of the layer of solid phase affected by an interface is approximately independent of the nature of the interface. This also would mean that the perturbed layer thickness is roughly independent of the interface energy, given that different interfaces have different free energies.

According to the findings mentioned above, the enthalpy content of the solid–liquid interface layer of thickness ξ_{min} should be equal to

$$h_{s,i}(T_m) = \frac{4}{3}\pi\left[(r-\delta)^3 - (r-\delta-\xi_{min})^3\right]\rho_s \Delta H_s(T_m) + 4\pi(r-\delta)^2 h_{sl}(T_m). \quad (12)$$

The corresponding $h_{s,i}(T_m)$ values are quoted in Fig. 9 as a function of the particle radius r together with the $s_{s,i}(T_m)$ ones. In both cases, the data show increasing trend. Correspondingly, the interface layers of the largest particles possess the largest enthalpy and entropy contents $h_{s,i}(T_m)$ and $s_{s,i}(T_m)$ because they are characterized by the smallest thickness ξ_{min} values. It appears therefore that the perturbation induced by the presence of a solid–liquid interface is restricted to layers with minimum thickness ξ_{min} becoming smaller and smaller as the particle radius r increases. Interface layers in relatively large particles seem therefore to sustain larger perturbations than smaller particles, where the perturbation is distributed over a more extended interface layer.

Conclusions

In summary, nanometer-sized particles undergo a two-stages solid–liquid phase transition. The first stage consists of a surface pre-melting process involving a relatively thin layer at the solid–vapor interface. The solid–liquid interface formed is stable within a certain temperature interval, thus permitting the coexistence of the solid particle interior and the molten surface layer. Finally, during the second stage of the particle melting process the solid–liquid interface propagates inward involving progressively larger regions of the particle interior. Both pre-melting and melting points are determined by the equality of free energy terms regarding interfaces and interiors. Whereas in the case of surface pre-melting the experimental data do not allow any reliable characterization of the process, the solid–liquid transformation of the particle interior can be satisfactorily described within the two-stages melting scenario. In particular, it appears that the depression of the latent heat of fusion is connected to the enthalpic contribution associated with the particle surface. This permits not only the estimation of the solid–liquid interface free energy, but also the distinction between its enthalpic and entropic terms.

The present work therefore shows that classical equilibrium thermodynamics provides an adequate and satisfactory theoretical framework for the rationalization of the melting behavior of nanometer-sized particles.

Acknowledgements Prof. L. H. Allen is acknowledged for having authorized the use of experimental data collected by his group at the Department of Materials Science and Engineering, University of Illinois at Urbana-Champaign. Financial support has been given by the University of Cagliari.

References

1. Alivisatos P (1996) Science 271:933
2. Moriarty P (2001) Rep Prog Phys 64:297
3. Jortner J, Rao CNR (2002) Pure Appl Chem 74:1491
4. Schmidt M, Kusche R, Von Issendorf B, Haberland H (1998) Nature 393:238
5. Thomson W (1871) Phil Mag 42:448
6. Pawlow P (1909) Z Phys Chem (Munich) 65:1
7. Hollomon TH, Turnbull D (1953) Progress in Metal Physics 4:333
8. Wronski CRM (1967) Brit J Appl Phys 18:1731
9. Coombes CJ (1972) J Phys F: Metal Phys 2:441
10. Baletto F, Ferrando R (2005) Rev Mod Phys 77:371
11. Buffat PH, Borel J-P (1976) Phys Rev A 13:2287
12. Couchman PR, Jesser WA (1977) Nature 269:481
13. Reiss H, Mirabel P, Whetten RL (1988) J Phys Chem 92:7241
14. Sakai H (1996) Surf Sci 351:285
15. Peters KF, Cohen JB, Chung Y-W (1998) Phys Rev B 57:13430
16. Tartaglino U, Zykova-Timan T, Ercolessi F, Tosatti E (2005) Phys Rep 411:291
17. Lai S, Guo JY, Petrova V, Ramanath G, Allen LH (1996) Phys Rev Lett 77:99
18. Efremov MYu, Schiettekatte F, Zhang M, Olson EA, Kwan AT, Berry LS, Allen LH (2000) Phys Rev Lett 85:3560
19. Zhang M, Efremov MYu, Schiettekatte F, Olson EA, Kwan AT, Lai SL, Greene JE, Allen LH (2000) Phys Rev B 62:10548
20. Olson EA, Efremov MYu, Zhang M, Zhang Z, Allen LH (2005) J Appl Phys 97:034304
21. Delogu F (2005) J Phys Chem B 109:21938
22. Brandes EA, Brook GB (eds) (1992) Smithells metals reference handbook, 7th edn. Butterworth-Heinemann, Oxford
23. Porter DA, Easterling KE (1992) Phase transformations in metals and alloys, 2nd edn. Chapman & Hall, London
24. Kauzmann W (1948) Chem Rev 43:219
25. Kleinert H (1989) Gauge theory in condensed matter. World Scientific, Singapore